Chinese Physics Letters

EXPRESS LETTER

Uncovering the Magnetization Multipolar Anisotropy of the Anomalous Hall Effect in Conventional Ferromagnets

Cite as: Wenzhi Peng *et al*. 2026 *Chin. Phys. Lett.* **43** 060704

DOI CSTR

Recommended Articles

Pressure-Tunable Large Anomalous Hall Effect in Ferromagnetic Metal $LiMn_6Sn_6$

Lingling Gao *et al*.
Chin. Phys. Lett. **41**, (2024)

Observation of Giant Topological Hall Effect in Room-Temperature Ferromagnet $Cr_{0.82}Te$

Wei-Ting Miao, Wei-Li Zhen, Zhen Lu, Heng-Ning Wang, Jie Wang, Qun Niu, and Ming-Liang Tian
Chin. Phys. Lett. **41**, (2024)

Unveiling of Terahertz Emission from Ultrafast Demagnetization and the Anomalous Hall Effect in a Single Ferromagnetic Film

Zhiqiang Lan, Zhangshun Li, Haoran Xu, Fan Liu, Zuanming Jin, Yan Peng, and Yiming Zhu
Chin. Phys. Lett. **41**, (2024)

Enhanced Anomalous Hall Effect of Pt on an Antiferromagnetic Insulator with Fully Compensated Surface

Yu Bai *et al*.
Chin. Phys. Lett. **39**, 108501 (2022)

Large Anomalous Hall Conductivity in Quasi-One-Dimensional Geometrically Frustrated Metal Pr_3MnBi_5

Xinyao Li, Feihong Guan, Xinhang Shan, Xiangde Zhu, Wei Ning, and Mingliang Tian
Chin. Phys. Lett. **43**, 040702 (2026)

Quantum Anomalous Hall Effects Controlled by Chiral Domain Walls

Qirui Cui, Jinghua Liang, Yingmei Zhu, Xiong Yao, and Hongxin Yang
Chin. Phys. Lett. **40**, (2023)

A series journal of Chinese Physical Society distributed by IOP Publishing

iopscience.iop.org/cpl | cpl.iphy.ac.cn

Chinese Physics Letters

Chin. Phys. Lett. **43** 060704 (2026)

EXPRESS LETTER

DOI: 10.1088/0256-307X/43/6/060704
CSTR: 32039.14.0256-307X.43.6.060704

Uncovering the Magnetization Multipolar Anisotropy of the Anomalous Hall Effect in Conventional Ferromagnets

Wenzhi Peng(彭文治)[1,†], Zheng Liu(刘正)[2,3,†], Haolin Pan(潘昊霖)[1], Peng Wang(王鹏)[1], Yulong Chen(陈昱龙)[1], Jiachen Zhang(张家晨)[1], Xuhao Yu(于绪昊)[1], Jinhui Shen(沈金辉)[1], Mingmin Yang(杨明敏)[4], Jiahao Han(憨家豪)[5], Qian Niu(牛谦)[2,3,*], Yang Gao(高阳)[1,2,3,*], and Dazhi Hou(侯达之)[1,2,*]

[1]International Center for Quantum Design of Functional Materials, School of Emerging Technology, University of Science and Technology of China, Hefei 230026, China
[2]Department of Physics, University of Science and Technology of China, Hefei 230026, China
[3]CAS Key Laboratory of Strongly-Coupled Quantum Matter Physics, University of Science and Technology of China, Hefei 230026, China
[4]Hefei National Laboratory, Hefei 230088, China
[5]Center for Science and Innovation in Spintronics, Tohoku University, Sendai, Japan

[†]These authors contributed equally to this work.
[*]Corresponding authors. Email: niuqian@ustc.edu.cn; ygao87@ustc.edu.cn; dazhi@ustc.edu.cn

The anomalous Hall effect (AHE) in ferromagnets is conventionally described by a dipolar relation between the anomalous Hall conductivity and the magnetization, which enforces their parallel alignment and thus forbids a Hall signal when the magnetization lies within the Hall plane. Here, by systematically measuring the AHE under in-plane magnetization in Fe and Ni, we uncover a multipolar anisotropy of the AHE that produces a finite in-plane anomalous Hall response in Fe(103) and Ni(111), while it vanishes in Fe(001) as dictated by crystal symmetry. The angular dependence of the in-plane AHE in Fe(103) and Ni(111) further deviates from the familiar sinusoidal form expected from dipolar behavior, revealing symmetry-allowed higher-order multipolar contributions. First-principles calculations quantitatively reproduce the experimentally extracted dipolar and octupolar coefficients for Fe, demonstrating that intrinsic Berry curvature carries a sizable multipolar anisotropy in conventional cubic ferromagnets.

The anomalous Hall effect (AHE) refers to the generation of a transverse potential difference in ferromagnetic conductors without an external magnetic field ($\boldsymbol{H}$), perpendicular to both the applied current ($\boldsymbol{J}_c$) and magnetization ($\boldsymbol{M}$) [1–11]. Pioneering studies revealed that the anomalous Hall resistivity (ρ_{xy}^{AHE}) shows a linear response to the out-of-plane magnetization (M_z) [1–7,12], which can be expressed as

$$\rho_{xy}^{\mathrm{AHE}} = R_s M_z, \tag{1}$$

where R_s is the coefficient of the AHE. This textbook knowledge focuses on the dipolar contribution of $\boldsymbol{M}$ to the anomalous Hall conductivity ($\boldsymbol{\sigma}^{\mathrm{AHE}}$), suggesting that $\boldsymbol{\sigma}^{\mathrm{AHE}}$ should be parallel to $\boldsymbol{M}$ [13]. This dipolar origin of the AHE dictates that the anomalous Hall signal vanishes when the $\boldsymbol{M}$ lies within the Hall plane, consistent with most studies on the AHE [1–7,14].

However, the AHE under in-plane magnetization was already observed in iron two decades ago [15,16], in apparent contradiction to Eq. (1) and therefore beyond the conventional dipolar framework. Although in-plane AHE can in principle arise from anisotropic $\boldsymbol{\sigma}^{\mathrm{AHE}}$ in $\boldsymbol{M}$ space in low-symmetry materials [17–22], such a mechanism is excluded in cubic ferromagnets such as Fe, where the dipolar framework predicts an isotropic $\boldsymbol{\sigma}^{\mathrm{AHE}}$ parallel to $\boldsymbol{M}$ [Fig. 1(a)] and thus a vanishing AHE for in-plane $\boldsymbol{M}$ [14]. Similar in-plane AHE has since been reported in other materials, including Fe_3Sn_3 [23] and $SrRuO_3$ [24], reinforcing the need for a framework beyond the dipolar description [see Section 2 in Supplementary Material (SM)]. Recently, Liu *et al.* developed a theory describing the AHE as a spin-group symmetry breaking phenomenon, which was further reformulated in terms of $\boldsymbol{M}$ multipoles that reflect the underlying AHE structure in $\boldsymbol{M}$ space [25–27]:

$$\rho_{xy}^{\mathrm{AHE}} = \overleftrightarrow{R}_s^{(2)} : \hat{M}\cdot\hat{z} + \sum_{N\geq 3}^{\mathrm{odd}} (\overleftrightarrow{R}_s^{(N+1)} : \overbrace{\hat{M}\hat{M}\cdots\hat{M}}^{N})\cdot\hat{z}. \tag{2}$$

Here, the leading term is the familiar dipolar contribution, whereas the second term contains the previously neglected higher-order multipolar contributions. Within this framework, the in-plane AHE originates from symmetry-allowed multipolar terms when the dipolar response is forbidden. While this theory captures the intrinsic contribution to the in-plane AHE, direct quantitative comparison between experimentally extracted multipolar coefficients and first-principles calculations remains lacking.

In this work, we fill this gap by quantitatively testing the multipolar framework through a direct comparison between experimentally extracted multipolar coefficients and first-principles calculations based on the Berry curvature multipoles in the $\boldsymbol{M}$ space. For materials with O_h point-group symmetry, such as Fe, Eq. (2) reduces to

$$\sigma_i^{\mathrm{AHE}} = \alpha m_i + \beta m_i^3 + \cdots, \tag{3}$$

where $\sigma_i^{\mathrm{AHE}} = \frac{1}{2}\epsilon_{ijk}\sigma_{jk}$, $\boldsymbol{m}$ is the unit vector of $\boldsymbol{M}$, and $i,j,k = x,y,z$ correspond to the (100), (010), and (001) directions, respectively. When only the linear term is retained, $\boldsymbol{\sigma}^{\mathrm{AHE}}$ remains isotropic and parallel to $\boldsymbol{M}$ [Fig. 1(a)], recovering the conventional dipolar framework. By contrast, the higher-order multipolar terms, exemplified by βm_i^3, introduce anisotropy into $\boldsymbol{\sigma}^{\mathrm{AHE}}$ [Fig. 1(b)], allowing an out-of-plane component of $\boldsymbol{\sigma}^{\mathrm{AHE}}$ to emerge even when $\boldsymbol{M}$ lies within the Hall plane and thereby producing an in-plane AHE [Fig. 1(c)]. For example, in an Fe(103) thin film, $\boldsymbol{M}$ aligned along $[30\bar{1}]$ induces $\boldsymbol{\sigma}^{\mathrm{AHE}}$ along $[27,0,\bar{1}]$, so that the octupolar term gives $\boldsymbol{\sigma}^{\mathrm{AHE}}$ an out-of-plane component and thereby generates a measurable in-plane AHE. This enables a quantitative determination of the leading dipolar and octupolar coefficients from the measured out-of-plane and in-plane AHE responses. The experimentally determined coefficients in Fe agree well with first-principles calculations, demonstrating that the in-plane AHE in conventional ferromagnets such as Fe originates predominantly from Berry-curvature multipoles in $\boldsymbol{M}$ space and further

Received 14 April 2026; accepted 24 April 2026; published 22 May 2026
© 2026 Chinese Physical Society and IOP Publishing Ltd. All rights, including for text and data mining, AI training, and similar technologies, are reserved.

Check for updates

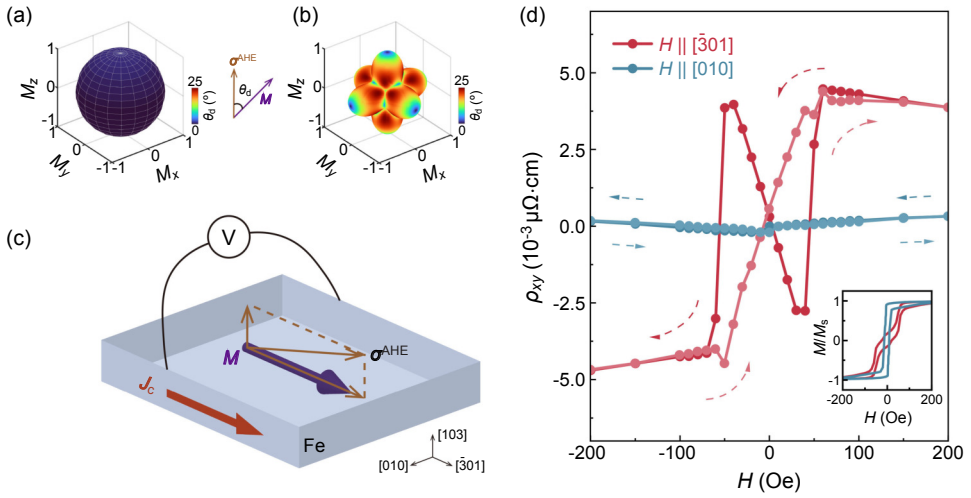

Fig. 1. The in-plane anomalous Hall Effect (AHE) originating from the $\boldsymbol{M}$ multipole. (a) and (b) Illustration of the (a) dipolar and (b) multipolar structures of the anomalous Hall conductivity ($\boldsymbol{\sigma}^{\rm AHE}$) in the O_h point group. The azimuthal angle and the radial length respectively denote the direction of $\boldsymbol{M}$ and the amplitude of the dipole and multipole terms. $\theta_{\rm d}$ denotes the offset angle between the direction of $\boldsymbol{\sigma}^{\rm AHE}$ and $\boldsymbol{M}$. The multipolar structure depicted in (b) is assumed mainly due to the octupolar contribution. (c) Schematic of the measurement for the in-plane AHE in Fe(103) film, where $\boldsymbol{M}$ and $\boldsymbol{J}_{\rm c}$ are both aligned in-plane along Fe[$\bar{3}$01]. The anomalous Hall signal can be observed due to the out-of-plane component of $\boldsymbol{\sigma}^{\rm AHE}$ induced by the $\boldsymbol{M}$ multipoles, even when $\boldsymbol{M}$ is in the Hall plane. (d) The in-plane AHE is observed in a 100 nm Fe(103) thin film when sweeping the magnetic field $\boldsymbol{H}$ along the Fe[$\bar{3}$01] (red curve), but is absent when $\boldsymbol{H}$ is aligned with Fe[010] (blue curve). The inset shows the $\boldsymbol{M}$–$\boldsymbol{H}$ curves with $\boldsymbol{H}$ sweeping along Fe[$\bar{3}$01] (red curve) and Fe[010] (blue curve).

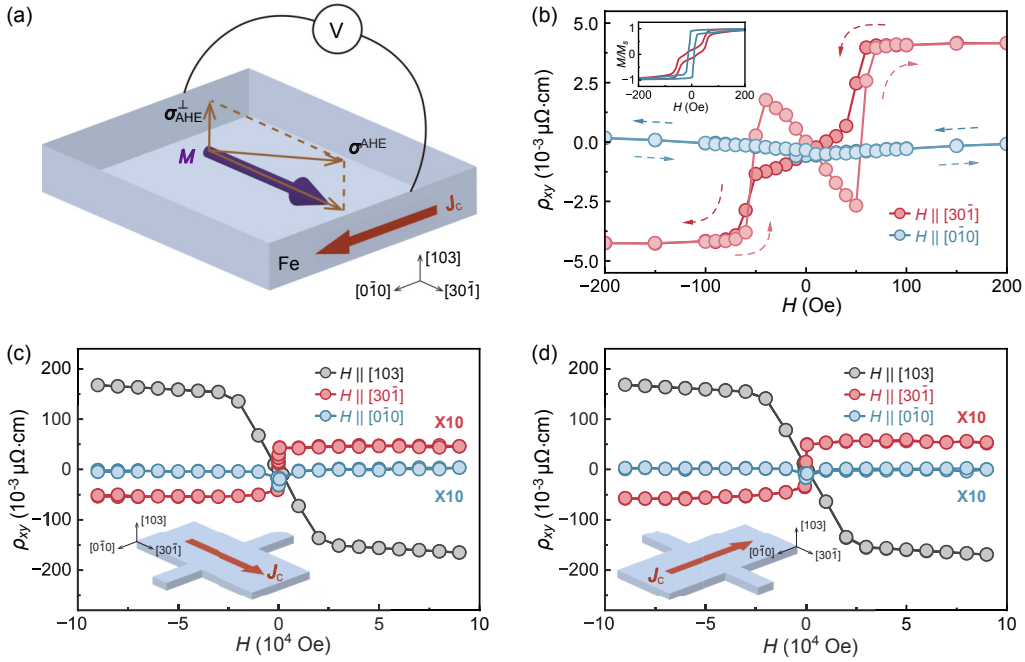

Fig. 2. Systematic measurement of the in-plane AHE in Fe(103) films. (a) Illustration of the Hall measurement for an Fe(103) thin film with a current applied along Fe[0$\bar{1}$0]. (b) Hall resistivity measured with $\boldsymbol{H}$ || Fe[30$\bar{1}$] and $\boldsymbol{H}$ || Fe[0$\bar{1}$0] for $|H| \le 200$ Oe at $T = 300$ K, and the inset depicts the $\boldsymbol{M}$–$\boldsymbol{H}$ curves measured for the two field orientations. An in-plane AHE signal is observed for $\boldsymbol{H}$ || Fe[30$\bar{1}$] but is absent for $\boldsymbol{H}$ || Fe[0$\bar{1}$0], mirroring the behavior shown in Fig. 1(d). (c) and (d) Hall resistivity measured at a magnetic field up to 90000 Oe with current applied along Fe[30$\bar{1}$] and Fe[0$\bar{1}$0], respectively, where the magnetic field is swept along the perpendicular and two in-plane directions.

revealing the multipolar anisotropy of the AHE predicted by theory [26,27].

The above scenario is directly observed in the experiment of Fig. 1(d), which plots the transverse resistivity (ρ_{xy}) of a 100 nm Fe(103) film versus the applied $\boldsymbol{H}$ at 300 K, measured with a charge current $\boldsymbol{J}_{\rm c}$ || Fe[$\bar{3}$01] [28]. The $\boldsymbol{H}$ dependence of the in-plane AHE coincides with the $\boldsymbol{M}$–$\boldsymbol{H}$ curve shown in the inset of Fig. 1(d). This result underscores its origin from the in-plane $\boldsymbol{M}$, consistent with the expected in-plane AHE depicted in Fig. 1(c). In contrast, the anomalous Hall signal is not observed for $\boldsymbol{H}$ || Fe[010], which can be understood by the collinear alignment between $\boldsymbol{\sigma}^{\rm AHE}$ and $\boldsymbol{M}$ dictated by the C_4 symmetry of the [010] axis (see Section 3 in SM).

Figure 2(a) depicts an alternative configuration for the Hall measurement, where the orientations of the applied current and the Hall probes are swapped in comparison to the arrangement shown in Fig. 1(c). Figure 2(b) shows the ρ_{xy} measured with $\boldsymbol{H}$ || Fe[$\bar{3}$01] and $\boldsymbol{H}$ || Fe[010]. The ρ_{xy} dependencies on $\boldsymbol{H}$ closely resembles those in Fig. 1(d), demonstrating that the Hall signal is primarily governed by the $\boldsymbol{M}$ direction rather than the $\boldsymbol{J}_{\rm c}$ direction [16,23,24]. It is worth noting that if the $\boldsymbol{M}$ is not fully aligned with the $\boldsymbol{H}$ during the in-plane field sweeping process, its out-of-plane component can also induce an anomalous Hall signal due to the linear $\boldsymbol{M}$ term in the

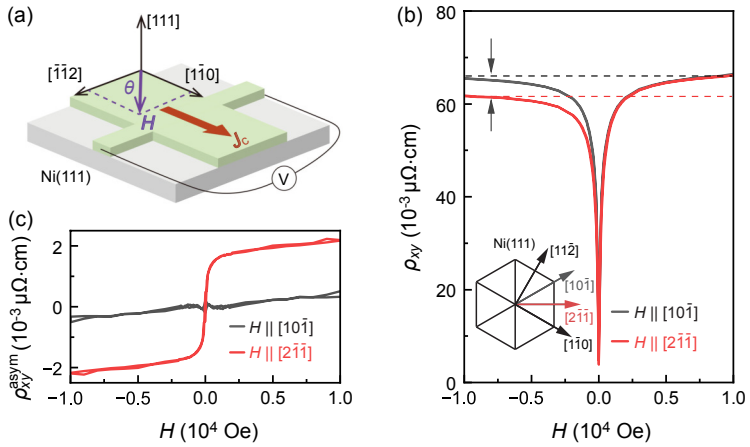

Fig. 3. Observation of the in-plane AHE in Ni. (a) Illustration of a Hall bar of Ni(111) thin film with a charge current along Ni[1$\bar{1}$0]. (b) Hall resistivity measured with $\boldsymbol{H}$ ∥ Ni[2$\bar{1}\bar{1}$] and $\boldsymbol{H}$ ∥ Ni[10$\bar{1}$] for $|H| \leq 10000$ Oe at $T = 300$ K, and the inset depicts the in-plane crystalline directions of Ni(111). Besides the similar symmetric contributions due to the planar Hall effect, an antisymmetric contribution is observed for $\boldsymbol{H}$ ∥ Ni[2$\bar{1}\bar{1}$] but is absent for $\boldsymbol{H}$ ∥ Ni[10$\bar{1}$]. (c) The field-asymmetric contribution extracted from (b), which reveals that a hysteresis-loop-like Hall signal is only observed for $\boldsymbol{H}$ ∥ Ni[2$\bar{1}\bar{1}$], consistent with the in-plane AHE induced by the AHE octupole.

AHE [29,30]. To discern whether the observed Hall signals in Figs. 1(d) and 2(b) are of such a trivial physical origin, we carried out Hall measurement in both setups at magnetic field of 90000 Oe in magnitude, with the result shown in Figs. 2(c) and 2(d). In both figures, the Hall signals remain constant with increasing in-plane magnetic field after saturation, distinct from the attenuation behavior of the AHE induced by the out-of-plane component of tilted magnetization as reported in Ref. [29,30]. When the magnetic field was aligned normal to the sample, the signal due to the conventional out-of-plane AHE can be observed.

The temperature dependence of the anomalous Hall conductivities for both out-of-plane AHE($\sigma_{\mathrm{OOP}}^{\mathrm{AHE}}$) and in-plane AHE($\sigma_{\mathrm{IP}}^{\mathrm{AHE}}$) in the Fe(103) thin film are shown in Fig. S3(a) of the SM. These distinct temperature dependencies further underscore different origins of the out-of-plane AHE and in-plane AHE. The observation of in-plane AHE in Fe challenges conventional dipolar framework but aligns well with the scenario involving $\boldsymbol{M}$ multipoles [26,27]. Notably, the multipolar framework not only explains the in-plane AHE observed in our Fe(103) films, but also accounts for similar phenomena recently reported in other ferromagnetic systems [23,24], thereby offering a unified perspective that reshapes the understanding of the AHE.

To quantitatively analyze this behavior, we consider to the octupolar term in Eq. (3), which reduces to $\sigma_i^{\mathrm{AHE}} = \alpha m_i + \beta m_i^3$. Here, the linear and cubic terms correspond to the dipolar and octupolar contributions, respectively, with $\alpha = p_{xx} - \frac{3}{2} o_{xxxx}$ and $\beta = \frac{5}{2} o_{xxxx}$, where p_{xx} and o_{xxxx} denote the symmetry-allowed dipolar and octupolar coefficients in Fe. The validity of this truncation is discussed in Section 3 of the SM. Combining the measurement of the longitudinal resistivity, the $\sigma_{\mathrm{OOP}}^{\mathrm{AHE}}$ and $\sigma_{\mathrm{IP}}^{\mathrm{AHE}}$ at 300 K are determined to be 1122 $\Omega^{-1}\cdot\mathrm{cm}^{-1}$ and $-34.5\,\Omega^{-1}\cdot\mathrm{cm}^{-1}$, respectively. Based on these results, the coefficients corresponding to the AHE dipole and octupole within Eq. (3) for Fe are determined as: $p_{xx} = 1153.7\,\Omega^{-1}\cdot\mathrm{cm}^{-1}$ and $o_{xxxx} = -57.5\,\Omega^{-1}\cdot\mathrm{cm}^{-1}$, respectively. On the theoretical front, we calculate the intrinsic $|\boldsymbol{\sigma}^{\mathrm{AHE}}|$ contributed from dipole and octupole terms using first-principles calculations [31], yielding: $p_{xx} = 922.8\,\Omega^{-1}\cdot\mathrm{cm}^{-1}$ and $o_{xxxx} = -54.7\,\Omega^{-1}\cdot\mathrm{cm}^{-1}$ (see Section 4 in SM). These theoretical values match well with our experimental results, further validating the Berry curvature multipolar origin of the AHE in ferromagnets.

Figure 3(a) shows the Hall measurement geometry for a Ni(111) film, in which an in-plane AHE is also observed. Although Ni(111) is a well-studied conventional ferromagnetic system [32–34], its Hall response under in-plane magnetization has remained largely unexplored [35]. As shown in Fig. 3(b), ρ_{xy} contains a pronounced field-symmetric planar Hall contribution for both $\boldsymbol{H}$ ∥ Ni[10$\bar{1}$] and $\boldsymbol{H}$ ∥ Ni[2$\bar{1}\bar{1}$], but a field-antisymmetric component appears only for the latter orientation. Figure 3(c) shows the extracted antisymmetric part, where a hysteresis loop is resolved only for $\boldsymbol{H}$ ∥ Ni[2$\bar{1}\bar{1}$], with a saturation field consistent with the corresponding $\boldsymbol{M}$–$\boldsymbol{H}$ curve. This orientation-selective in-plane AHE cannot be accounted for within the conventional dipolar picture, but follows naturally from the higher-order multipolar anisotropy of the AHE, which can generate an out-of-plane component of $\boldsymbol{\sigma}^{\mathrm{AHE}}$ for some in-plane magnetization directions but not for others. The observation of this behavior in both Fe and Ni indicates that the in-plane AHE is a general manifestation of multipolar AHE anisotropy in conventional ferromagnets.

A quantitative analysis analogous to that for Fe can likewise be carried out for Ni. From the measured out-of-plane and in-plane AHE, we extract $p_{xx} = 610.5\,\Omega^{-1}\cdot\mathrm{cm}^{-1}$ and $o_{xxxx} = -79.0\,\Omega^{-1}\cdot\mathrm{cm}^{-1}$, yielding a ratio $|o_{xxxx}/p_{xx}| \approx 0.13$ that is notably larger than that in Fe (∼0.05). This indicates a relatively stronger octupolar contribution in Ni, in line with the Berry curvature multipole picture, in which the octupole appears as a higher-order term in the spin–orbit coupling expansion and thus becomes relatively more pronounced as the spin–orbit coupling strengthens. Since Ni has a larger atomic number Z than Fe, and the spin–orbit coupling generally scales approximately as Z^4, the enhanced octupolar-to-dipolar ratio in Ni is naturally understood within this framework [36].

Figures 4(a) and 4(b) depict the experimental setup for measuring the magnetization angle dependence of the Hall signal for Fe(103) and Ni(111) films. The magnitude of $\boldsymbol{H}$ is set at 10000 Oe to ensure that the magnetization is saturated and parallel to $\boldsymbol{H}$ throughout the rotation process. Figure 4(c) shows the field angle dependence of ρ_{xy} in a 100 nm Fe(103) film, encompassing contributions from both the planar Hall effect (PHE) and the in-plane AHE [37–41]. Owing to its even parity in relation to magnetization, the PHE signal is evident as even harmonics of the field angle θ. Conversely, the in-plane AHE, with its odd parity concerning magnetization, should be characterized by odd harmonics of θ. We employ Fourier expansion to extract the odd and even harmonic constituents of the ρ_{xy}–θ curve in Fig. 4(c), as plotted in Figs. 4(d) and 4(e), respectively. The field angle dependence of the in-plane AHE significantly diverges from the commonly observed $\sin\theta$ characteristic in the previous AHE studies [14,42–44]. Figure 4(f) shows the field angle dependence of ρ_{xy} in an 80 nm Ni(111) film. Figure 4(g) shows the odd harmonic component of the curve in Fig. 4(f) which manifests a three-fold angle dependence, and Fig. 4(h) shows a typical planar Hall behavior as in Fig. 4(e). We further carried out the same in-plane field rotation measurement of ρ_{xy} in a 100 nm Fe(001) film, and the results are shown in Fig. S4 of the SM in which the in-plane AHE was not found. These findings reveal qualitative differences in the in-plane AHE behaviors across samples with

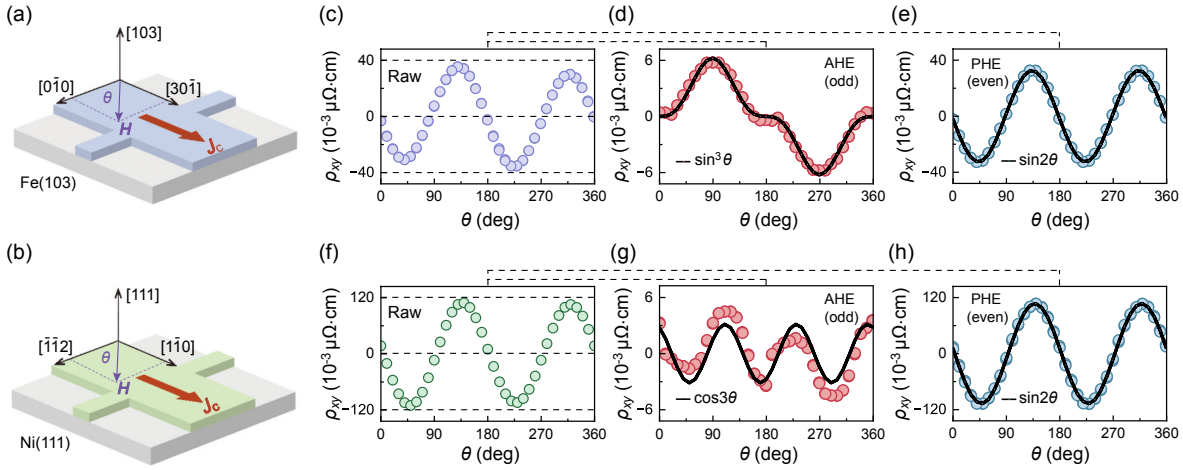

Fig. 4. Magnetization orientation dependences of the in-plane AHE. (a) and (b) Illustrations for the Hall measurement with rotating in-plane magnetic field $\boldsymbol{H}$ for Fe(103) and Ni(111) films, respectively. The magnitude of the magnetic field is set at 10000 Oe, which is sufficiently strong to align $\boldsymbol{M}$ parallel to $\boldsymbol{H}$. (c) Field angle dependence of the Hall resistivity in a 100 nm Fe(103) film. (d) and (e) The contributions from odd harmonics and even harmonics derived from (c), respectively. The odd-harmonic pattern agrees well with Eq. (4) predicted by the AHE octupole. The even-harmonic contribution displays a sin2θ dependence due to the planar Hall effect. (f) Field angle dependence of the Hall resistivity in a 80 nm Ni(111) film. (g) The odd-harmonic components in (f), which shows a three-fold field angle dependence with a comparable magnitude as in (d), consistent with Eq. (5) predicted by the AHE octupole. (h) The even-harmonic components in (f), showing a sin2θ dependence due to the planar Hall effect.

varying crystalline orientations, which calls for a unified theoretical exploration to elucidate this unconventional behavior not observed in prior AHE researches.

Now we are in a position to derive the magnetization angle dependence of the in-plane AHE from Eq. (3), and it is insightful to start from the symmetry analysis of the AHE octupole. Based on Eq. (3), when the magnetization direction varies on a Bloch sphere, the anomalous Hall conductivity can have a nontrivial landscape determined by the crystalline symmetry. With only the dipole term, the AHE is always isotropic in cubic crystals and the Hall deflection plane is always perpendicular to the magnetization. In contrast, the octupole term allows the magnetization lying in the Hall deflection plane to induce a Hall signal as demonstrated in this work.

In Fe(103) films, when we rotate the $\boldsymbol{M}$ within the (103) plane by an angle θ with respect to the Fe[010], the corresponding magnetization direction can be expressed as: $\hat{m}_x = -\sin\theta\cos\phi$, $\hat{m}_y = \cos\theta$, and $\hat{m}_z = \sin\theta\sin\phi$, with ϕ representing the angle between the (103) and (001) plane. By substituting $\hat{m}_i$ into Eq. (3) and isolating the component perpendicular to the (103) plane, we obtain

$$|\boldsymbol{\sigma}^{\perp}_{\mathrm{AHE}}|_{\mathrm{Fe(103)}} = \frac{6}{25}\beta_{\mathrm{Fe}}\sin^3\theta, \tag{4}$$

which yields an excellent match with the AHE data in Fig. 4(d) using just a single adjustable parameter. Similarly, we obtain the magnetization angle dependence of $|\boldsymbol{\sigma}^{\perp}_{\mathrm{AHE}}|$ in Ni(111) by applying the same derivation:

$$|\boldsymbol{\sigma}^{\perp}_{\mathrm{AHE}}|_{\mathrm{Ni(111)}} = \frac{\sqrt{2}}{6}\beta_{\mathrm{Ni}}\cos(3\theta), \tag{5}$$

which explains the three-fold symmetry of the in-plane AHE data in Fig. 4(g). Additionally, the analysis of Fe(001) reveals that $|\boldsymbol{\sigma}^{\perp}_{\mathrm{AHE}}|_{\mathrm{Fe(001)}}$ vanishes, elucidating the absence of in-plane AHE in Fe(001) films. Thus we reach a comprehensive understanding of the different magnetization angle dependencies of the in-plane AHE in Fe and Ni films, which are essentially different manifestation of the AHE octupole.

The above analysis is based on the ideal crystallographic symmetry of Fe and Ni and identifies the angular dependence expected from the AHE octupole. In real epitaxial films, lattice mismatch with the substrate may introduce residual strain and lower the crystal symmetry [14,16], allowing an additional anisotropic dipolar contribution to the in-plane AHE [45,46]. XRD and reciprocal space mapping measurements on the 100 nm Fe(103) film indeed reveal a weak strain-induced distortion (Fig. S1 in SM), so such a dipolar-like term can in principle exist. Moreover, a slight tilt of $\boldsymbol{M}$ out of the Hall plane may also generate a first-harmonic contribution originating from the much larger out-of-plane AHE [29,30]. Nevertheless, these dipolar-like contributions are contained in the first harmonic, whereas the octupolar term has a distinct third-harmonic component. Fourier expansion therefore separates these contributions: the extracted octupolar contribution is 6.2×10^{-3} μΩ·cm, while the remaining first-harmonic term is only 2.0×10^{-4} μΩ·cm (Fig. S3 in SM). Thus, strain-induced symmetry lowering and tilt-related effects provide only minor corrections, and the in-plane AHE is dominated by the multipolar anisotropy discussed above.

The present work establishes a quantitative paradigm for identifying Berry curvature multipoles through transport: the in-plane AHE directly probes the higher-order multipolar anisotropy of the AHE, and its combination with the out-of-plane AHE enables quantitative extraction of the multipolar coefficients. This framework is broadly applicable, since our symmetry analysis shows that the AHE octupole in magnetization space is permissible across all Bravais lattices. For example, the hexagonal D_6 lattice hosts two independent nonzero coefficients o_{ijkl}, while the tetragonal D_4 and C_{4v} lattices host three and the orthorhombic D_2 lattice hosts six [26]. This implies richer anisotropic Hall responses and a more readily observable in-plane AHE in lower-symmetry materials. Guided by these symmetry considerations, our analysis identifies several two-dimensional ferromagnets, including $CrTe_2$, $Cr_2Ge_2Te_6$, and $CrSiTe_3$ [47–51], as promising candidates that satisfy the symmetry criteria for an in-plane AHE driven by AHE octupoles. Beyond ferromagnets, an in-plane AHE has recently been reported in the antiferromagnet $Mn_3Ni_{0.35}Cu_{0.65}N$ and interpreted in terms of its noncollinear magnetic structure [52], which may also be captured within the AHE octupole framework. It should be emphasized that symmetry analysis determines only which multipolar coefficients are allowed, not their magnitudes. The relative strength of the dipolar and multipolar terms is governed by microscopic mechanisms, including the intrinsic Berry curvature multipolar contribution in magnetization space and extrinsic scattering processes [16,26]. Within the Berry curvature multipole framework, the multipolar contributions generally emerge as higher-order terms in the perturbative expansion with respect to spin-orbit coupling, and are therefore naturally expected to be smaller than the leading dipolar contribution [26]. This expectation is consistent with the in-plane AHE observed so far, which remains substantially weaker than the out-of-plane AHE across a variety of systems [16,23,24].

The observation of the in-plane AHE due to the AHE octupole

underscores the significance of the distribution of geometric quantities such as the Berry curvature within the magnetization space, highlighting a paradigm shift from the traditional focus on geometric influences in real and momentum spaces [6,10,53]. Based on the concept of the octupole in the magnetization space, additional in-plane Hall-type effects could be discovered. For instance, the anomalous Nernst effect, anomalous Ettinghausen effect, and anomalous thermal Hall effect—each a divergent branch from the AHE [54–57]—it is plausible to expect their in-plane counterparts due to the octupole contribution within suitable ferromagnets. Theoretically, there exists substantial intrigue in discussing the criteria essential for optimizing the octupole contribution and its extended effects across diverse systems. Collectively, these emerging effects due to octupole in the magnetization space may constitute a novel classification of physical phenomena, expanding our understanding and offering new perspectives and paradigms in the study of condensed matter physics.

Author Contributions

W.P. and D.H. designed the experiment and analysed the data. W.P., H.P., and M.Y. fabricated the samples and performed characterization of the sample. W.P. carried out the electric measurement. Z.L., W.P., D.H., Q.N., and Y.G. developed the explanation of the experiment. W.P., J.H., and D.H. wrote the manuscript. P.W., Y.C., J.Z., X.Y., and J.S. helped the experiment. All authors discussed the results and commented on the manuscript.

Competing Interests

The authors declare that they have no competing interests.

Acknowledgments

This work was supported by the National Natural Science Foundation of China (Grant Nos. 12234017, 12074366, and 12374164). D. Hou and Y. Gao were supported by the Fundamental Research Funds for the Central Universities (Grant Nos. WK9990000116 and WK2340000102). Z. Liu was supported by the National Natural Science Foundation of China (Grant Nos. 11974327 and 12004369), the Fundamental Research Funds for the Central Universities (Grant Nos. WK3510000010 and WK2030020032), the Anhui Initiative in Quantum Information Technologies (Grant No. AHY170000), and the Innovation Program for Quantum Science and Technology (Grant No. 2021ZD0302800). The set-up of magnetic sputtering system and thin film growth was assisted by Anhui Epitaxy Technology Co., Ltd. The sample fabrication was supported by the USTC Center for Micro- and Nanoscale Research and Fabrication. The authors thank S. Yang, Z.G. Liang, and L.F. Wang for the magnetization measurement. The authors thank B. Wan for the TEM measurement.

References

[1] Hall E H 1880 *Proc. Phys. Soc. London* **4** 325
[2] Nagaosa N, Sinova J, Onoda S, MacDonald A H, and Ong N P 2010 *Rev. Mod. Phys.* **82** 1539
[3] Dheer P N 1967 *Phys. Rev.* **156** 637
[4] Jungwirth T, Sinova J, Wang K Y, Edmonds K W, Campion R P, Gallagher B L, Foxon C T, Niu Q, and MacDonald A H 2003 *Appl. Phys. Lett.* **83** 320
[5] Tian Y, Ye L, and Jin X F 2009 *Phys. Rev. Lett.* **103** 087206
[6] Nakatsuji S, Kiyohara N, and Higo T 2015 *Nature* **527** 212
[7] Liu E K, Sun Y, Kumar N, Muechler L, Sun A L, Jiao L, Yang S Y, Liu D F, Liang A J, Xu Q N, Kroder J, Suss V, Borrmann H, Shekhar C, Wang Z S, Xi C Y, Wang W H, Schnelle W, Wirth S, Chen Y L, Goennenwein S T B, and Felser C 2018 *Nat. Phys.* **14** 1125
[8] Luttinger J M 1958 *Phys. Rev.* **112** 739
[9] Berger L 1970 *Phys. Rev. B* **2** 4559
[10] Chen H, Niu Q, and MacDonald A H 2014 *Phys. Rev. Lett.* **112** 017205
[11] Shi G, Zhang M J, Yan D Y, Feng H L, Yang M, Shi Y G, and Li Y Q 2020 *Chin. Phys. Lett.* **37** 047301
[12] Zeng C G, Yao Y G, Niu Q, and Weitering H H 2006 *Phys. Rev. Lett.* **96** 037204
[13] Roman E, Mokrousov Y, and Souza I 2009 *Phys. Rev. Lett.* **103** 097203
[14] Chen H R, Cheng Z, Feng Y Z, Xu H Y, Wu T, Chen C H, Chen Y, Yuan Z, and Wu Y Z 2025 *Phys. Rev. B* **111** 014437
[15] Friedland K J, Nötzel R, Schönherr H P, Riedel A, Kostial H, and Ploog K H 2001 *Physica E* **10** 442
[16] Chen H R, Cui Y W, Wu T, Wu Y Z, Pei K, Wang Y X, Chen Y, Xu H Y, Che R C, Yuan Z, Xiao C, and Wu Y Z 2025 *Phys. Rev. B* **111** 174423
[17] Tan H X, Liu Y Z, and Yan B H 2021 *Phys. Rev. B* **103** 214438
[18] Zhang H B, Blügel S, and Mokrousov Y 2011 *Phys. Rev. B* **84** 024401
[19] Zhang Y P and Zhang C W 2011 *Phys. Rev. B* **84** 085123
[20] Liu X, Hsu H C, and Liu C X 2013 *Phys. Rev. Lett.* **111** 086802
[21] Ren Y F, Zeng J J, Deng X Z, Yang F, Pan H, and Qiao Z H 2016 *Phys. Rev. B* **94** 085411
[22] Zhong P C, Ren Y F, Han Y L, Zhang L Y, and Qiao Z H 2017 *Phys. Rev. B* **96** 241103
[23] Wang L J Y, Zhu J J, Chen H Y, Wang H, Liu J J, Huang Y X, Jiang B Y, Zhao J J, Shi H J, Tian G, Wang H Y, Yao Y G, Yu D P, Wang Z W, Xiao C, Yang S A, and Wu X S 2024 *Phys. Rev. Lett.* **132** 106601
[24] Nishihaya S, Matsuki Y, Kaminakamura H, Sugeno H, Jiang M C, Murakami Y, Arita R, Ishizuka H, and Uchida M 2025 *Adv. Mater.* **37** e02624
[25] Liu P F, Li J Y, Han J Z, Wan X G, and Liu Q H 2022 *Phys. Rev. X* **12** 021016
[26] Liu Z, Wei M J, Peng W Z, Hou D Z, Gao Y, and Niu Q 2025 *Phys. Rev. X* **15** 031006
[27] Liu Q H 2025 *Physics* **18** 127
[28] Peng W Z, Chen Y L, Yu X H, and Hou D Z 2023 *Materials* **16** 4352
[29] You Y R, Gong Y Y, Li H, Li Z F, Zhu M M, Tang J X, Liu E K, Yao Y G, Xu G Z, Xu F, and Wang W H 2019 *Phys. Rev. B* **100** 134441
[30] Tang J X, Xu G Z, You Y R, Xu Z, Zhang Z, Chen X, Gong Y Y, and Xu F 2020 *Appl. Phys. Lett.* **117** 202402
[31] Yao Y G, Kleinman L, MacDonald A H, Sinova J, Jungwirth T, Wang D S, Wang E G, and Niu Q 2004 *Phys. Rev. Lett.* **92** 037204
[32] Ibach H and Bruchmann D 1980 *Phys. Rev. Lett.* **44** 36
[33] Meyer A, Flege J I, Rettew R E, Senanayake S D, Schmidt T, Alamgir F M, and Falta J 2010 *Phys. Rev. B* **82** 085424
[34] Lalmi B, Girardeaux C, Portavoce A, Ottaviani C, Aufray B, and Bernardini J 2012 *Phys. Rev. B* **85** 245306
[35] Philippi-Kobs A, Farhadi A, Matheis L, Lott D, Chuvilin A, and Oepen H P 2019 *Phys. Rev. Lett.* **123** 137201
[36] Koseki S, Matsunaga N, Asada T, Schmidt M W, and Gordon M S 2019 *J. Phys. Chem. A* **123** 2325
[37] Tang H X, Kawakami R K, Awschalom D D, and Roukes M L 2003 *Phys. Rev. Lett.* **90** 107201
[38] Lin T, Tang C, Alyahayaei H M, and Shi J 2014 *Phys. Rev. Lett.* **113** 037203
[39] Nandy S, Sharma G, Taraphder A, and Tewari S 2017 *Phys. Rev. Lett.* **119** 176804
[40] Hua E D, Dai K J, Wang Q, Ye H, Liu K, Zhang J F, Lu J D, Liu K, Jin F, Wang L F, and Wu W B 2023 *Chin. Phys. Lett.* **40** 077501
[41] Cai M J, Chen Z, Yang Y, Zhu X D, Sun H X, Zhu A K, Liu X, Han Y Y, Gao W S, and Tian M L 2024 *Chin. Phys. Lett.* **41** 077303
[42] Limmer W, Glunk M, Daeubler J, Hummel T, Schoch W, Sauer R, Bihler C, Huebl H, Brandt M S, and Goennenwein S T B 2006 *Phys. Rev. B* **74** 205205
[43] Wang Y S, Lee P A, Silevitch D M, Gomez F, Cooper S E, Ren Y, Yan J Q, Mandrus D, Rosenbaum T F, and Feng Y J 2020 *Nat. Commun.* **11** 216
[44] Guillet T, Marty A, Vergnaud C, Jamet M, Zucchetti C, Isella G, Barbedienne Q, Jaffrès H, Reyren N, George J M, and Fert A 2021 *Phys. Rev. B* **103** 064411
[45] Zhou J D, Zhang W J, Lin Y C, Cao J, Zhou Y, Jiang W, Du H F, Tang B J, Shi J, Jiang B Y, Cao X, Lin B, Fu Q D, Zhu C, Guo W, Huang Y Z, Yao Y G, Parkin S S P, Gao Y, Wang Y J, Hou Y, Suenaga K, Wu X S, and Liu Z 2022 *Nature* **609** 46
[46] Cui Y W, Li Z Q, Chen H R, Wu Y Z, Chen Y, Pei K, Wu T, Xie N, Che R C, Qiu X P, Liu Y, Yuan Z, and Wu Y Z 2024 *Sci. Bull.* **69** 2362
[47] Sun X D, Li W Y, Wang X, Sui Q, Zhang T Y, Wang Z, Liu L, Li D, Feng S, Zhong S Y, Wang H W, Bouchiat V, Nunez Regueiro M,

Rougemaille N, Coraux J, Purbawati A, Hadj-Azzem A, Wang Z H, Dong B J, Wu X, Yang T, Yu G Q, Wang B W, Han Z, Han X F, and Zhang Z D 2020 *Nano Res.* **13** 3358

[48] Miao W T, Zhen W L, Lu Z, Wang H N, Wang J, Niu Q, and Tian M L 2024 *Chin. Phys. Lett.* **41** 067501

[49] Meng K, Li Z Y, Shen Y C, Bi X Y, Rao J H, Qian Y T, Gao Z S, Chen P, Qiu C Y, Qin F, Wu J X, Luo F, Huang J W, and Yuan H T 2024 *Chin. Phys. Lett.* **41** 097501

[50] Fang Y M, Wu S Q, Zhu Z Z, and Guo G Y 2018 *Phys. Rev. B* **98** 125416

[51] Casto L D, Clune A J, Yokosuk M O, Musfeldt J L, Williams T J, Zhuang H L, Lin M W, Xiao K, Hennig R G, Sales B C, Yan J Q, and Mandrus D 2015 *APL Mater.* **3** 041515

[52] Rajan A, Saunderson T G, Lux F R, Díaz R Y, Abdullah H M, Bose A, Bednarz B, Kim J Y, Go D, Hajiri T, Shukla G, Gomonay O, Yao Y G, Feng W X, Asano H, Schwingenschlögl U, López-Díaz L, Sinova J, Jakob G, Mokrousov Y, Manchon A, and Kläui M 2026 *Commun. Mater.* **7** 73

[53] Fang Z, Nagaosa N, Takahashi K S, Asamitsu A, Mathieu R, Ogasawara T, Yamada H, Kawasaki M, Tokura Y, and Terakura K 2003 *Science* **302** 92

[54] Li X K, Xu L C, Ding L C, Wang J H, Shen M S, Lu X F, Zhu Z W, and Behnia K 2017 *Phys. Rev. Lett.* **119** 056601

[55] Qian Y T, Zhang J Y, Bi X Y, Chen P, Cao H Z, Xu W F, Liu Z Y, Zhai K, Yuan H T, and Huang J W 2025 *Chin. Phys. Lett.* **42** 090713

[56] Li Y H, Huang S, Zhu W, Pan C, Gong P W, Zhang J W, and Qiu X P 2026 *Chin. Phys. Lett.* **43** 020708

[57] Seki T, Iguchi R, Takanashi K, and Uchida K 2018 *Appl. Phys. Lett.* **112** 152403